EVALUATION OF CFD MODELS FOR SOLID-PROPELLANT ROCKET-EXHAUST MODELING

Dana Mikkelsen[1]

[1]University of Central Florida, Orlando, FL, 32816

ABSTRACT

Particulate flow is often simulated using one of two numerical methods: Euler-Lagrange and Euler-Euler. The Eulerian-Lagrangian method analyzes the particulate phase as a control mass, which is solved alongside the Eulerian equations for the continuous phase. This method models particulate behavior with a high degree of accuracy, but a large amount of computing power may be required. The Eulerian-Eulerian method analyzes a control volume, treating both the particulate phase and the continuous phase as continuous fluid. In this method, the particulate is solved as continuous. Thus, the effects of the individual particles are not modeled accurately. The aim is to determine which method is more efficient at modeling a 2D simulation of a rocket jet impinging on a normal surface. In this study, Computational Fluid Dynamics (CFD) is used to evaluate flow characteristics of a rocket jet using both Euler-Lagrange and Euler-Euler numerical methods.

NOMENCLATURE

F = force ***[N]***
F_D = drag force ***[N]***
F_L = lift force ***[N]***
C_D = drag coefficient
M = sum of inertial forces and momentum transfer associated with mass transfer
a = acceleration $\boldsymbol{[m \cdot s^{-2}]}$
g = gravity acceleration $\boldsymbol{[m \cdot s^{-2}]}$
m = mass ***[kg]***
$\dot{m}$ = mass transfer rate $\boldsymbol{[kg \cdot s^{-1}]}$
N = total number of phases
p = pressure ***[Pa]***
Q = interfacial heat transfer
Re = Reynolds number
T = temperature ***[K]***
u = velocity $\boldsymbol{[m \cdot s^{-1}]}$
h = enthalpy $\boldsymbol{[J \cdot kg^{-1}]}$
d = particle diameter ***[m]***
r = jet radius ***[m]***
r_t = nozzle throat radius ***[m]***

Greek letters

α = volume fraction
ρ = density $\boldsymbol{[kg \cdot m^{-3}]}$
λ = thermal conductivity $\boldsymbol{[W \cdot m^{-1} \cdot K^{-1}]}$
σ_h = the turbulent thermal diffusion Prandtl number
τ = shear stress tensor $\boldsymbol{[kg \cdot m^{-1} \cdot s^{-2}]}$

Subscript

i = axis index
p = particle
t = turbulent

1. INTRODUCTION

NASA's upcoming SLS launch system is powered by two different types of engines. The main engines are four Aerojet Rocketdyne RS-25 engines. These engines are 'liquid engines,' using liquid hydrogen (LH2) as fuel and liquid oxygen (LOX) as the oxidizer [1]. In order to turn the gaseous hydrogen and oxygen into liquids, they are super-cooled and subjected to high pressures. These liquid propellants need special handling, and they evaporate at ambient temperatures and pressures.

In order to supplement the liquid engines, NASA uses two 'solid rocket boosters.' These rockets use aluminum powder (Al) for fuel and ammonium perchlorate (NH4ClO4) as the oxidizer. The two are bound together with polybutadiene acrylonitrile (PBAN). These solid materials are much more stable than the liquid materials in the RS-25 engine, thereby requiring less specialized handling and allowing them to sit longer before ignition. When ignited, the aluminum and the ammonium perchlorate react with each other and produce aluminum oxide (Al2O3), aluminum chloride (AlCl3), water vapor (H2O), and nitrogen gas (N2) [2].The presence of these solid particle products complicates the simulation and flow analysis of solid rockets, as the particulate creates a multi-phase flow.

2. BACKGROUND

There are two common numerical strategies utilized for the analysis of multi-phase flows: The Euler-Euler method and the Euler-Lagrange method. The Euler-Euler method analyzes a control volume, treating the particulate phase and the continuous phase as interacting continuous fluids [3, 4]. Assuming Newtonian fluid flow, unsteady state, compressible flow, and two-way coupling, the Euler-Euler approach is solved using mass conservation (Eq. 1), momentum balance (Eq. 2), and energy conservation (Eq. 4) for both the gas phase and the particulate phase.

$$\frac{\partial}{\partial t}\alpha_k\rho_k + \nabla\cdot\alpha_k\rho_k u_k = \sum_{j=1}^{N}(\dot{m}_{jk} - \dot{m}_{kj}) \ldots (1)$$

$$\frac{\partial}{\partial t}\alpha_k\rho_k u_k + \nabla\cdot\alpha_k\rho_k u_k^2 = -\alpha_k\nabla p + \alpha_k\rho_k g + \nabla\cdot\alpha_k(\tau_k + \tau_k^t) + M_k \ldots (2)$$

$$M = F_D + F_L + \sum_{j=1}^{N}(\dot{m}_{jk}u_j - \dot{m}_{kj}u_k) \ldots (3)$$

$$\frac{\partial}{\partial t}(\alpha_k\rho_k h_k) + \nabla\cdot(\alpha_k\rho_k u_k h_k) - \nabla\cdot\left[\alpha_k\left(\lambda_k\nabla T_k + \frac{\mu_t}{\sigma_h}\nabla h_k\right)\right] = Q_k \ldots (4)$$

The Euler-Lagrange method analyzes the particulate phase as a control mass, in which the force balance on each particle (Eq. 5) is solved alongside the Eulerian equations for the continuous phase [5, 6].

$$\frac{du_{i_p}}{dt} = F_D(u_i - u_{i_p}) + \frac{g_i(\rho_p - \rho)}{\rho_p} \ldots (5)$$

$$F_D = \frac{18\mu C_D Re}{24\rho_p d_p^2} \ldots (6)$$

Each method has its advantages and disadvantages. Lagrangian methods better represent the behavior of the individual particles, but often have a high computational cost and break down near the injector [6, 7]. Eulerian methods do not require the solving of individual particles, but do not model the particulate phase as accurately [2, 7].

Most numerical simulations of multi-phase flows (both Eulerian and Lagrangian) have dealt with subsonic flows. The purpose of this research is to determine which method is more efficient, which method is more accurate, and which method is the best for simulating hypersonic flows.

3. MATERIALS AND METHODS

The converging-diverging jet model used for this research was based on the dimensions of the Aerojet Rocketdyne RS-25 engine. The RS-25 is a liquid jet, not a solid rocket, so the rocket modeled in Star CCM+ is of an arbitrary geometry on the scale of the rockets used in the space program. The nozzle geometry can be found in Figure 1.

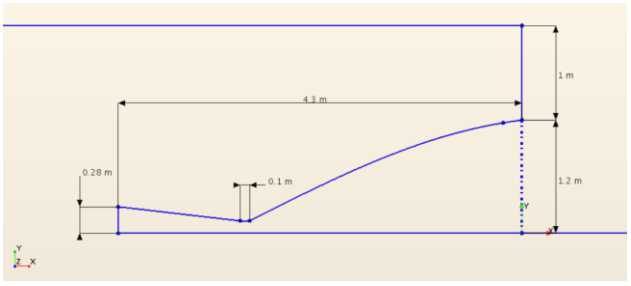

Fig. 1 Rocket Nozzle Geometry

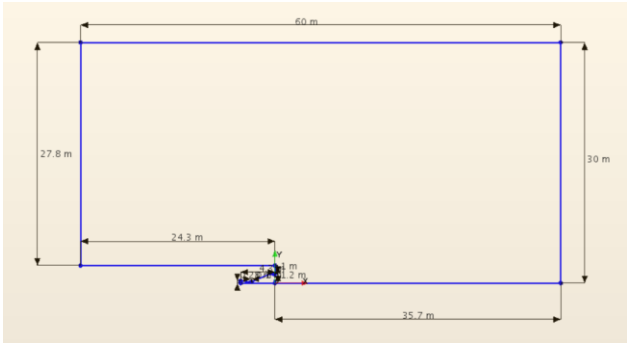

Fig. 2 Test Chamber Geometry

The test chamber geometry is outlined in Figure 2. The nozzle inlet was set as a stagnation inlet with a pressure of 1.52 x 10^6 Pa (15 atm) [8]. The lower bound of the model was set as a symmetry boundary. The upper bound of the nozzle and the flat boundary above it were set as walls. The far right boundary was set as an impinging wall. This wall was located 40 m from the nozzle inlet, approximately the distance to the bottom of NASA's flame trench. The top and leftmost boundaries were set as pressure outlets. These conditions applied to both the Eulerian and Lagrangian models.

It was hypothesized that either the Euler-Euler or the Euler-Lagrange model would be the superior method for modeling hypersonic particulate flow. The following studies (mesh sensitivity, Euler vs Lagrange, drag coefficient, and coupling) were conducted using 2D simulations.

Euler-Euler Model

The basic Euler-Euler model was built in Star CCM+ with the following physics models:

- Axisymmetric
- Coupled Energy
- Coupled Flow
- Dispersed Multiphase
    - Eulerian Phases
        - Constant Density
        - Flow Model
        - Liquid
        - Segregated Fluid Temperature
- Exact Wall Distance
- Gas
- Gradients
- Ideal Gas
- Implicit Unsteady
- K-Epsilon Turbulence
- Multiphase Interaction
    - Phase Interactions
        - DMP-Physics Continuum
        - Drag Force
        - Heat Transfer
        - Interaction Length Scale
- Realizable K-Epsilon Two-Layer
- Reynolds-Averaged Navier-Stokes
- Turbulent
- Two-Layer All y+ Wall Treatment

The density of the liquid was set to that of aluminum, 2700 kg/m^3, and the particle diameter was set as 1 x 10^{-5} m. The volume fraction of the Eulerian phase was 10%. The drag force coefficient used was Schiller-Naumann.

Certain Euler-Euler simulations were executed with the implicit unsteady solver, while others were executed as steady simulations.

Euler-Lagrange Model

The basic Euler-Lagrange model was built in Star CCM+ with the following physics models:

- Axisymmetric
- Coupled Energy
- Coupled Flow
- Exact Wall Distance
- Gas
- Gradients
- Ideal Gas
- Implicit Unsteady
- K-Epsilon Turbulence
- Lagrangian Multiphase
    - Lagrangian Phases
        - Constant Density
        - Drag Force
        - Pressure Gradient Force
        - Solid
        - Spherical Particles
        - Track File
- Realizable K-Epsilon Two-Layer
- Reynolds-Averaged Navier-Stokes
- Turbulent
- Two-Layer All y+ Wall Treatment

The solid was set as aluminum (Al). A particle injector was also created for the Euler-Lagrange model. The injector was a part injector located at the inlet. The particle diameter was set as a normal distribution with a standard deviation of 1.0 with a minimum diameter of 1.7 x 10^{-6} m and a maximum diameter of 3.3 x 10^{-6} m [9]. The mean diameter size was set as 2.5 x 10^{-6} m. The velocity used was 82.6 m/s and the volume flow rate was 1.1068 m^3/s.

Four line probes were set in each model at 5 m (Line Probe 1), 15 m (Line Probe 2), 25 m (Line Probe 3), and 35 m (Line Probe 4). These line probes measured velocity, pressure, Mach number, and volume fraction. The data from these line probes were compiled in a table and exported into plots. These plots were imported into Excel for analysis.

Mesh Sensitivity Study

Each model was tested with three different mesh densities. The ‘standard’ mesh (Fig. 3) had 7,775 cells; 15,274 faces; and 8065 vertices. The ‘coarse’ mesh (Fig. 4) had 3,003 cells; 5841 faces; and 3268 vertices. The ‘fine’ mesh (Fig. 5) had 23,828 cells, 47,121 faces; and 24,361 vertices. The ‘Standard Eulerian (Steady) simulation was run on a mesh similar to the Standard Mesh, but with an increase in boundary layers on the impinging wall (Fig. 6). It had 8,432 cells, 16,579 faces, and 8,730 vertices.

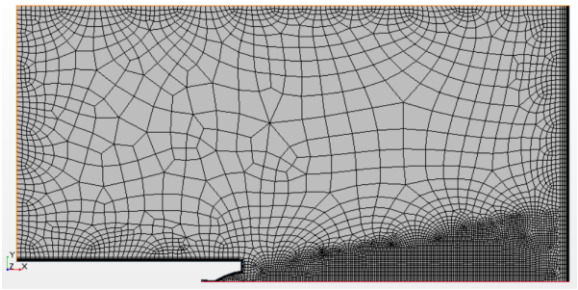

Fig. 3 Standard Mesh

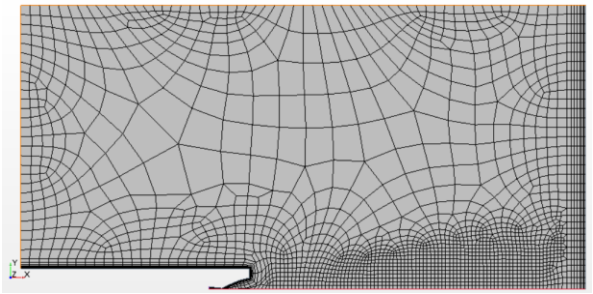

Fig. 4 Coarse Mesh

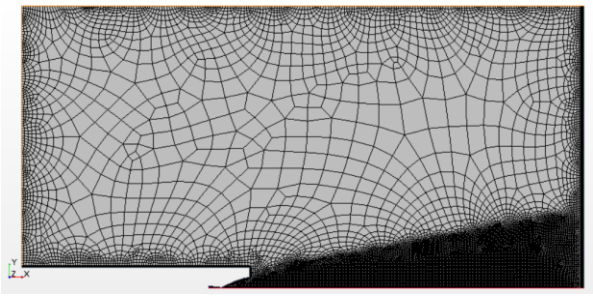

Fig. 5 Fine Mesh

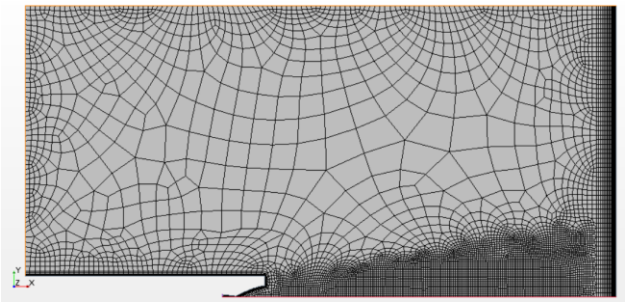

Fig. 6 'Steady Eulerian' Mesh

The time step utilized varied between models depending on the demands of the simulations, as did the number of maximum iterations. The maximum physical time was kept constant at 10 s, but the number of time steps completed in each simulation varied. These values can be found in Table A1.

The Euler-Euler and the Euler-Lagrange simulations were each run on all three meshes. The Euler-Euler simulations on the 'standard Eulerian' and 'fine' meshes were run as steady simulations; the first to investigate the differences between a steady and an unsteady simulation, and the second because the unsteady simulation would not converge.

Drag Coefficient Study

For the drag coefficient study, the drag coefficient for the Euler-Euler simulation run on the 'fine' mesh was changed from a Schiller-Naumann coefficient, which is unaffected by relative velocity [10] to a Loth correlation field function (Fig. A1), which took into account compressible flow effects [11]. The results of the simulation with the altered drag coefficient were then compared to the results of the simulation run with the Schiller-Naumann drag coefficient.

Coupling Study

In the coupling study, the 'fine mesh' Euler-Euler simulation was executed with the model 'Two-Way Coupling' selected. This model allows the particulate phase to affect the gas phase in addition to the gas phase affecting the particulate phase. The results from this simulation were compared to those of the simulation run with one-way coupling, in which the gas phase affected the particulate phase, but the particulate phase did not affect the gas phase

An attempt was made to rerun the Euler-Lagrange simulation with two-way coupling, but it refused to converge due to the sheer number of particles being analyzed.

4. RESULTS AND DISCUSSION

Mesh Sensitivity Study

As velocity, pressure, and Mach number are related, the results for velocity are the only ones discussed in this report. Each velocity profile was taken from Line Probe 2, 15m from the nozzle exit. The results of the mesh sensitivity study can be found in Figure 7 (Euler-Euler) and Figure 8 (Euler-Lagrange).

For both the Euler-Euler and Euler-Lagrange simulations, the velocity at the center of the jet flow increased with mesh refinement. This increase indicated that the mesh was not independent, or that the mesh refinement affected the flow results. The increase between the 'Standard Lagrange' and 'Fine Lagrange' simulations was minimal, indicating an independent mesh had been achieved and any further refinement would not affect the results of the simulation. This independence was not achieved with the Euler-Euler mesh.

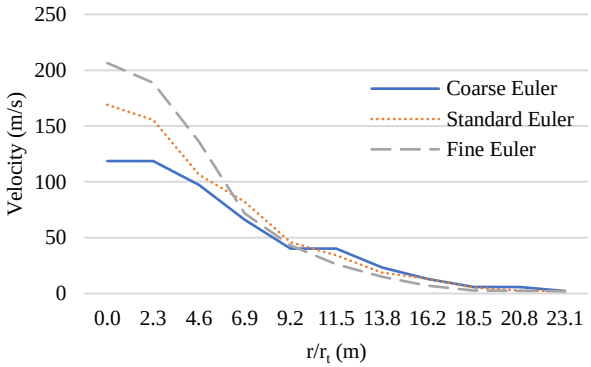

Fig. 7 Euler-Euler Velocity Profiles

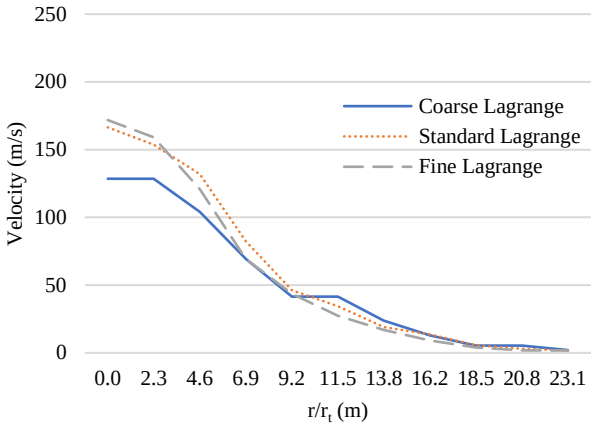

Fig. 8 Euler-Lagrange Velocity Profiles

The largest difference between each simulation was found at the center of the flow ($r/r_t = 0$). This was expected, as the unsteady flow is most strongly concentrated at the center and less so toward the boundary.

It is evident that the 'Fine Euler' flow was approximately 50m/s faster at the center of the flow than the 'Fine Lagrange' simulation. The Euler-Lagrange simulations were run as time-dependent, implicit unsteady simulations, while the Euler-Euler simulations were run as steady simulations. Due to this, the Euler-Lagrange simulation may not have achieved a steady solution. If it were run for another 10s, the results from the Euler-Lagrange simulation may change to better match those of the Euler-Euler simulation.

Each Euler-Lagrange simulation was run with differing time steps due to the demands of the mesh the simulation was run on. This difference in time step also affected the results of the Euler-Lagrange simulations. In order to achieve true steady-state results, a time average of the velocities could be taken along the flow over time.

The number of times steps the Euler-Lagrange simulations ran for also differed between meshes. Despite this difference, the line probe obtained a good temporal result as it captured data at a single instant in time. More time was needed for the simulations on the finer meshes to run, as they required a smaller time step.

Computational Time Study

The effects of mesh density on computational time were also studied. Unfortunately, each simulation was run with differing Max Time Steps and differing Max Inner Iterations (Table A1), so these results are not entirely accurate. Despite this, some trends in the data can be identified.

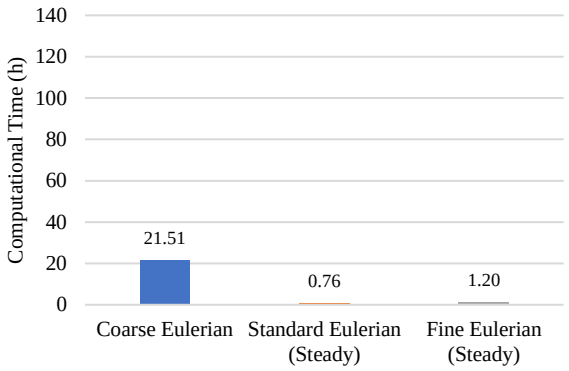

Fig. 9 Euler-Euler Computational Times

Running simulations as steady simulations instead of time-dependent implicit unsteady simulations had great effect on computational time, as evidenced in Fig. 9. The steady solution calculated only the final result, requiring less computational power than the implicit unsteady solution, which calculated the result at each individual time-step.

The 'Standard Eulerian (Steady)' simulation was originally run to use as comparison with a standard mesh unsteady Euler-Euler simulation, but there was an error with the unsteady simulation and the data was unusable. The 'Fine Eulerian (Steady)' simulation was run because an unsteady simulation on the fine mesh would not converge.

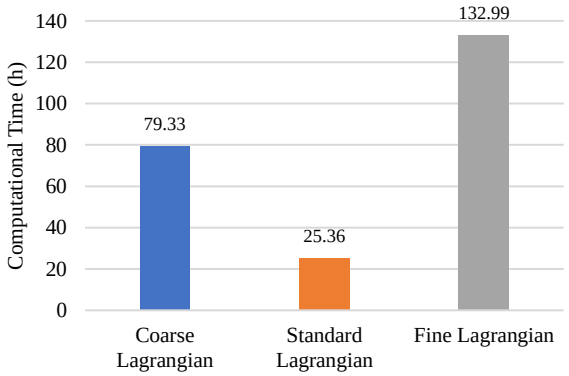

Fig. 10 Euler-Lagrange Computational Times

Overall, the Euler-Euler simulations (Fig. 9) required less computational time than the Euler-Lagrange simulations (Fig. 10). This was due to the Euler-Euler simulations solving only the three control-volume equations. The Euler-Lagrange simulations solved a mass balance for each particle on top of the control-volume equations.

One can see a general trend of finer meshes requiring increased computational time, which is expected. A finer mesh results in a higher number of cells to solve for. The 'Coarse Lagrangian' simulation having a higher computational time than the 'Standard Lagrangian'

simulation does not fit this trend, but that may be due to the disparity in runtimes between the two simulations (Table A2).

Drag Coefficient Study

The Schiller-Naumann drag coefficient, which was used for the simulations in this research, is a drag coefficient that is unaffected by relative velocity [10]. The Loth correlation field function, on the other hand, considers compressible effects [11].

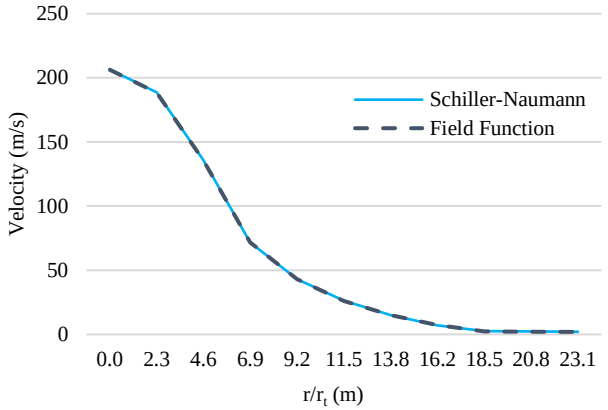

Fig. 11 Drag Coefficient Euler-Euler Velocity Profiles

It is evident in Figure 11 that this change in drag coefficient had essentially zero effect on the radial velocity profile of the jet flow. This negligible change indicates that the compressible effects of the flow were low.

Coupling Study

When the coupling model was changed from 1-way to 2-way coupling, the initial velocity of the gas phase decreased dramatically (Fig. 12). This was due to the fact the presence of the particles in the flow reduced the velocity of the gas flow as per Newton's second law (Eq. 7).

$$F = m \cdot a \ldots \textbf{(7)}$$

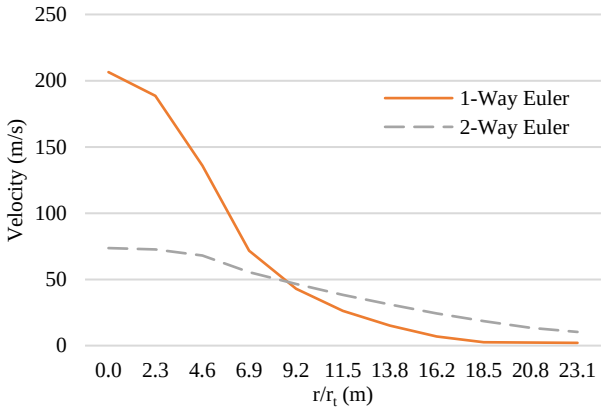

Fig. 12 1- & 2-Way Coupled Euler-Euler Velocity Profiles

At $r/r_t = 9.2$, the magnitude of the gas velocity of the 2-way coupled flow becomes greater than that of the 1-way coupled flow. This was expected, as the particle phase may affect the velocity of the flow at the boundary layer, accelerating the flow at the boundary layer while decelerating the center of the flow.

5. CONCLUSION

Despite some differences in the modeling strategies, some conclusions can be drawn. The Euler-Lagrange model reached mesh independence sooner than the Euler-Euler model, but the Euler-Euler model required less computational time, especially when run as a steady simulation. In addition, computational time increased as the mesh density increased.

As the difference between the simulation run with the Schiller-Naumann drag coefficient and the simulation run with the Loth correlation drag coefficient was negligible, the compressible effects of the flow were low.

The effect of 1- vs 2-way coupling was significant. The velocity at the center of the flow of the 2-way coupled model was 150 m/s slower than the velocity at the center of the 1-way coupled model. The velocity of the 2-way coupled flow at the boundary of the jet was slightly higher than that of the 1-way coupled model due to the effects of the particles and Newton's second law.

There is more research to be done on this topic. The simulations should be run again with standardized stopping criteria to get an accurate measure of the difference in computational time. Work needs to be done regarding the volume fractions of the particulate in each flow, and further analysis of the volume-averaged line probe profiles should be conducted. Most importantly, this computational data needs to be compared to data collected from actual experiments in order to verify its accuracy.

ACKNOWLEDGEMENTS

The researcher would like to acknowledge the National Science Foundation, the Department of Defense, and the University of Central Florida for making this research possible. In addition, she would like to thank Dr. Michael Kinzel and Dr. Douglas Fontes for providing support and direction in this research, Dr. Ali Gordon and Dr. Jeffrey Kauffman for organizing this REU HYPER summer program, and Robert Burke for answering questions and communicating information.

REFERENCES

[1] Perry, B., "We've Got (Rocket) Chemistry, Part 1," *Rocketology: NASA's Space Launch System* Available: https://blogs.nasa.gov/Rocketology/2016/04/15/weve-got-rocket-chemistry-part-1/.

[2] Perry, B., "We've Got (Rocket) Chemistry, Part 2," *Rocketology: NASA's Space Launch System* Available: https://blogs.nasa.gov/Rocketology/2016/04/21/weve-got-rocket-chemistry-part-2/.

[3] Patankar, N. A., and Joseph, D. D., "Modeling and numerical simulation of particulate flows by the Eulerian–Lagrangian approach," *International Journal of Multiphase Flow*, vol. 27, 2001, pp. 1659–1684.

[4] Vujanovic, M., Petranovic, Z., Edelbauer, W., Baleta, J., and Duic, N., "Numerical modelling of diesel spray using the Eulerian multiphase approach," *Energy Conversion and Management*, Mar. 2015, pp. 160–169.

[5] Gerber, A. G., "Two-Phase Eulerian/Lagrangian Model for Nucleating Steam Flow," *Journal of Fluids Engineering*, vol. 124, 2002, pp. 465–475.

[6] Apte, S. V., Gorokhovski, M., and Moin, P., "LES of atomizing spray with stochastic modeling of secondary breakup," *International Journal of Multiphase Flow*, vol. 29, Jun. 2003, pp. 1503–1522.

[7] Murrone, A., and Villedieu, P., "Numerical Modeling of Dispersed Two-Phase Flows," *AerospaceLab*, Mar. 2011, pp. 1–13.

[8] Zhukov, V. P., "The impact of methane oxidation kinetics on a rocket nozzle flow," *Acta Astronautica*, vol. 161, Jan. 2019, pp. 524–530.

[9] Hovland, D. L., "Particle Sizing in Solid Rocket Motors," *Naval Postgraduate School*, Mar. 1989, pp. 1-110.

[10] Schiller, L. and Naumann, Z., "A Drag Coefficient Correlation," *VDI Zeitung*, vol. 77, 1935, pp. 318-320.

[11] Loth, E., "Compressibility and Rarefaction Effects on Drag of a Spherical Particle," *AIAA Journal*, vol. 46-9, Sep. 2008, pp. 2219-2228.

APPENDIX

Figure A1 Loth Correlation Drag Coefficient Field Function

```
phase1_S_Al_CD      max(24./$phase1_S_Al_Rep*(1.0+0.15*pow($phase1_S_Al_Rep,0.687))*
                    $phase1_S_Al_HM+0.42*$phase1_S_Al_CM/(1.0+42000.*$phase1_S_Al_GM/
                    pow($phase1_S_Al_Rep,1.16)),0.1)

phase1_S_Al_CM      $phase1_S_Al_Mp<1.45 ? 5./3.+2./3.*tanh(3.*log($phase1_S_Al_Mp+
                    0.1)) : 2.044 + 0.2*exp(-1.8*log(pow($phase1_S_Al_Mp/1.5,2)))

phase1_S_Al_GM      $phase1_S_Al_Mp<0.89 ? 1-1.525*pow($phase1_S_Al_Mp,4) : 0.0002+
                    0.0008*tanh(12.77*($phase1_S_Al_Mp-2.02))

phase1_S_Al_HM      1.0-0.258*$phase1_S_Al_CM/(1.0+514.*$phase1_S_Al_GM)

phase1_S_Al_Mp      mag($$phase1_S_Al_Vslip)/$SoundSpeed

phase1_S_Al_momFlux $${VelocityParticulate}[0]*$VolumeFractionParticulate*
                    ${DensityParticulate}

phase1_S_Al_Rep     max(${PhasePairReynoldsNumberPhase Interaction 1},1.e-4)

phase1_S_Al_Vslip   $${Velocity}-$${VelocityParticulate}
```

Table A1 Simulation Settings

	Simulation Settings					
	Coarse Eulerian	Coarse Lagrangian	Standard Eulerian	Standard Lagrangian	Fine Eulerian	Fine Lagrangian
Max Inner Iterations	60	30	20	30	30	15
Max Time Steps	90000	70000	30000	30000	30000	60000
Δt	1e-4	1e-3		1e-3		1e-4
# Iterations	2249940	1020030	19250	607995	26856	949740

Table A2 Simulation Statistics

	Simulation Statistics (s)					
	Coarse Eulerian	Coarse Lagrangian	Standard Eulerian	Standard Lagrangian	Fine Eulerian	Fine Lagrangian
Max Physical Runtime	10	10	2	10	10	10
Physical Runtime	3.600630	10		10.00024		5.39214
Iteration CPU Time	0.034964	0.015513	1.29	0.061252	0.161056	0.106998
CPU Time per Time Step	2.019382	7.167536		1.995745		9.102091
Total CPU Time	77424.2138	285578.9917	2723.338	91293.734	4324.073304	478779.5528
Total CPU Time (h)	**21.507**	**79.327**	**0.756**	**25.359**	**1.201**	**132.994**